Published in final edited form as:

Eur Radiol. 2018 January ; 28(1): 331–339. doi:10.1007/s00330-017-4962-1.

Amide proton transfer imaging for differentiation of benign and atypical meningiomas

Bio Joo, MD[1], **Kyunghwa Han, PhD**[2], **Yoon Seong Choi, MD, PhD**[2], **Seung-Koo Lee, MD, PhD**[2], **Sung Soo Ahn, MD, PhD**[2,*], **Jong Hee Chang, MD, PhD**[3], **Seok-Gu Kang, MD, PhD**[3], **Se Hoon Kim, MD, PhD**[4], and **Jinyuan Zhou, PhD**[5]

[1]Department of Radiology, The Armed Forces Capital Hospital, Gyeonggi-do, Korea

[2]Department of Radiology and Research Institute of Radiological Science, College of Medicine, Yonsei University College of Medicine, Seoul, Korea

[3]Department of Neurosurgery, Yonsei University College of Medicine, Seoul, Korea

[4]Department of Pathology, Yonsei University College of Medicine, Seoul, Korea

[5]Division of MRI Research, Department of Radiology, Johns Hopkins University School of Medicine, Baltimore, Maryland, United States

Abstract

Purpose—To investigate the difference in amide proton transfer (APT)-weighted signals between benign and atypical meningiomas and determine the value of APT imaging for differentiating the two.

[*]Address correspondence to: Sung Soo Ahn, MD, PhD, Assistant Professor, Department of Radiology, College of Medicine, Yonsei University, 50 Yonsei-ro, Seodaemun-gu, Seoul 120-752, Korea, Phone: +82-2-2228-7400, Fax: +82-2-393-3035, SUNGSOO@yuhs.ac.

Compliance with ethical standards:

Guarantor:
The scientific guarantor of this publication is Seung-Koo Lee, M.D., Ph.D.

Conflict of interest:
The authors of this manuscript declare no relationships with any companies, whose products or services may be related to the subject matter of the article.

Statistics and biometry:
One of the authors has significant statistical expertise.
Kyunghwa Han, PhD,
Department of Radiology and Research Institute of Radiological Science, College of Medicine, Yonsei University College of Medicine, Seoul, Korea

Informed consent:
Written informed consent was waived by the Institutional Review Board.

Ethical approval:
Institutional Review Board approval was obtained.

Methodology:

- retrospective
- diagnostic or prognostic study
- performed at one institution

Methods—Fifty-seven patients with pathologically diagnosed meningiomas (benign, 44; atypical, 13), who underwent preoperative MRI with APT imaging between December 2014 and August 2016 were included. We compared normalized magnetization transfer ratio asymmetry ($nMTR_{asym}$) values between benign and atypical meningiomas on APT-weighted images. Conventional MRI features were qualitatively assessed. Both imaging features were evaluated by multivariable logistic regression analysis. The discriminative value of MRI with and without $nMTR_{asym}$ was evaluated.

Results—The $nMTR_{asym}$ of atypical meningiomas was significantly greater than that of benign meningiomas (2.46% vs. 1.67%; $P < 0.001$). In conventional MR images, benign and atypical meningiomas exhibited significant differences in maximum tumour diameter, non-skull base location, and heterogeneous enhancement. On multivariable logistic regression analysis, high $nMTR_{asym}$ was an independent predictor of atypical meningiomas (adjusted OR, 11.227; $P = 0.014$). The diagnostic performance of MRI improved with $nMTR_{asym}$ for predicting atypical meningiomas.

Conclusion—Atypical meningiomas exhibited significantly higher APT-weighted signal intensities than benign meningiomas. The discriminative value of conventional MRI improved significantly when combined with APT imaging for diagnosis of atypical meningioma.

Keywords

Meningioma; Magnetic resonance imaging; Tumour grading; Chemical exchange saturation transfer (CEST); Amide proton transfer (APT)

Introduction

With advances in imaging techniques and knowledge of tumour microenvironment, chemical exchange saturation transfer (CEST) was proposed as a novel magnetic resonance imaging (MRI) technique for detecting endogenous mobile proteins and peptides, even at relatively low molecular concentrations [1]. Amide proton transfer (APT) imaging is a specific form of CEST imaging based on chemical exchange of amide protons without exogenous contrast agents [2–5]. Here, exchangeable labile solute protons in amide bonds are selectively saturated by 3.5-ppm downfield off-resonance radiofrequency (RF) irradiation and transferred to bulk water by proton exchange, leading to a discernible decrease in signal intensity in bulk water and, eventually, to image contrast [4]. This technique has been successfully applied in human brain imaging for several diseases, including tumours and stroke [5–9]. Although the origin of APT signals in tumours is controversial, previous studies have suggested an increase in APT-weighted signals within brain tumours, especially in malignant tumours, due to increased mobile protein concentrations in malignant cells, associated with increased cellularity [2, 3, 5, 6, 9–11].

Intracranial meningioma is a common primary brain tumour in adults [12, 13]. A majority of meningiomas are benign (World Health Organization [WHO] grade I) and have favourable prognosis. However, nearly 10% of meningiomas are atypical (WHO grade II) or malignant (WHO grade III) tumours with aggressive biological behaviour, a tendency to recur [14], and, consequently, relatively worse prognosis, as evident from 5-year survival rates of 67.5%

and 60% for patients with Grade II and III meningiomas, respectively [15]. In routine clinical practice, surgical resection followed by adjuvant radiotherapy is considered for treatment of atypical/malignant meningioma, especially in cases involving subtotal resection [16]. Preoperative prediction of meningioma grade is important because it influences treatment planning, including the surgical resection strategy. For differentiating between benign and atypical/malignant meningiomas, several conventional MRI findings have been suggested as indicators of aggressive tumours, including non-skull base location, T2 hyperintensity, peritumoural brain oedema, indistinct tumour-brain interface, irregular tumour margins, heterogeneous tumour enhancement, capsular enhancement, cystic changes, and skull invasion [17–23]. These findings, however, are not sufficiently reliable for grading meningiomas to ensure proper treatment planning. Although several studies have investigated the feasibility of APT imaging for grading glial tumours [9, 24], to the best of our knowledge, no study has employed APT imaging for grading meningiomas. Therefore, this study aimed to investigate the differences in APT-weighted signal between benign and atypical meningiomas and determine the value of APT imaging for differentiating the two.

Materials and Methods

Study Population

This retrospective study was approved by the institutional review board, and the requirement for informed consent was waived. Sixty consecutive patients with pathologically diagnosed meningiomas, who underwent preoperative MRI including APT and conventional imaging between December 2014 and August 2016, were enrolled. We excluded three patients because of poor image quality due to the susceptibility effect or patient motion (n = 2) and inadequate lesion size for image analysis (n = 1). Thus, 57 patients (male, 16; female, 41; mean age 54.4 ± 12.4 years) were included in this study. The interval between MRI and surgery was less than 3 days for all patients.

MRI Protocol

Imaging studies were performed with a 3T MRI system (Achieva TX, Philips) using a 32-channel receiver head coil and a transmitter body coil. Conventional MR images were acquired according to the standard extra-axial brain tumour protocol in our hospital, which involves the following: (a) T2-weighted imaging (T2WI) in all three orthogonal directions; (b) axial T1-weighted imaging; and (c) three-dimensional (3D) contrast-enhanced T1WI. Additionally, APT images were acquired before contrast administration using the 3D gradient- and spin-echo approach [25] with the following imaging parameters: acquisition voxel size, 2.2 × 2.2 mm; slice thickness, 4.4 mm; TR/TE, 3000/17 ms; turbo spin-echo factor, 22; echo planar imaging factor, 7; and number of slices to cover the entire tumour, 15. Six saturation frequency offsets (±3.0, ±3.5 and ±4.0 ppm) were adopted, with four repetitions at ±3.5 ppm, to attain sufficient signal-to-noise ratio within the clinical time frame [5, 24]. Images were acquired with an RF saturation amplitude of 2 μT and total duration of 800 ms, with a four-block pulsed saturation scheme. Water-frequency shift due to field inhomogeneity was measured in a separate image acquired using the water-saturation shift referencing method with 21 offset frequencies ranging from -1.25 to 1.25 ppm, at intervals of 0.125 ppm (16 Hz), with one reference image acquired without a

saturation RF pulse, resulting in a full Z-spectrum within the offset range [26]. The water-saturation shift reference image was acquired with a TR/TE of 1250/17 ms, RF saturation amplitude of 0.5 μT, and total duration of 400 ms, with a two-block pulsed saturation scheme. The total acquisition time for both APT and water-saturation shift reference images was 7 min 36 s.

APT Image Processing

After APT and water-saturation shift reference images were obtained, water frequency shift correction was performed. The full water-saturation shift Z-spectrum was fitted by a 12^{th} order polynomial on voxel-by-voxel basis for all offset frequencies. The fitted curve was then interpolated at a higher spectral resolution (1 Hz), where the lowest signal in the fit after interpolation was assumed to be an actual water resonance frequency. The water centre frequency offset was set as the measured displacement between the actual and ideal the water resonance frequency (0 Hz). The acquired APT-weighted data at the saturation frequency offsets (±3.0, ±3.5, ±4.0 ppm) were interpolated over the offset range and shifted using the estimated water centre frequency offset to obtain final shift-corrected APT-weighted image data [26]. Based on the shift-corrected data, magnetization transfer ratio asymmetry (MTR_{asym}) values at ± 3.5 ppm with respect to water frequency were calculated [4]:

$$MTR_{asym}\,(+3.5ppm) = \frac{S_{sat}\,(-3.5ppm) - S_{sat}\,(+3.5ppm)}{S_0}$$

where S_0 and S_{sat} (±3.5 ppm) are MRI signals without and with saturation RF pulse, respectively. APT-weighted images were then generated using MTR_{asym} at 3.5 ppm. All data processing was performed offline, using Matlab (MathWorks, Natick, MA).

Image Analysis

Circular regions of interest (ROIs) were drawn on APT-weighted images, which were independently evaluated by two neuroradiologists (with 8 and 3 years of experience in neuroradiology) blinded to clinical and histopathological data. First, three circular ROIs were manually placed in different slices on raw APT images which exhibited similar contrast with T2WI for anatomical landmarks in the brain. Each ROI was located in a place that best represented the entire tumour signal. We carefully attempted to exclude cystic or necrotic portions referring to both T2WI and post-contrast T1WI and included the area with the highest signal within tumours. Another ROI was placed in normal-appearing white matter (NAWM). Then, the ROIs were transferred to processed APT-weighted images (Fig 1). The measured signal intensities in the three ROIs within tumour on processed APT-weighted images were averaged to represent the tumour. Thus, mean MTR_{asym} values for solid enhancing tumours and NAWM were obtained in each patient. Finally, normalized MTR_{asym} ($nMTR_{asym}$) values were calculated as follows:

$$nMTR_{asym} = MTR_{asym}\,(\text{tumor}) - MTR_{asym}\,(\text{NAWM})$$

where MTR_{asym} (tumour) is the mean MTR_{asym} of ROIs in enhancing tumours, and MTR_{asym} (NAWM) is the mean MTR_{asym} of ROIs in corresponding NAWM. The ROIs ranged in size from 518.4 to 691.2 mm^2. The mean MTR_{asym} values of the two readers were used for further analysis.

Conventional MR images were analysed for tumour location, maximum tumour diameter, T2 hyperintensity, peritumoural brain oedema, irregular tumour margin, heterogeneous enhancement, capsular enhancement, cystic changes, hyperostosis of adjacent skull, skull invasion, and the dural tail sign by the same two neuroradiologists. Tumour location was categorized as “skull base” or “non-skull base.” T2 hyperintensity was defined as higher signal intensity of the tumour relative to grey matter on T2WI. Irregular tumour margin was defined by the lobulated appearance of tumour margins on contrast-enhanced T1WI. The mean values of maximum tumour diameters measured by the two neuroradiologists were determined for further analysis. Discrepancies were settled by consensus between the two radiologists.

Surgery and Pathological Evaluation

All patients underwent surgical tumour resection after MRI. Pathological diagnosis was made by neuropathologists according to the WHO criteria. Criteria for atypical meningioma (WHO grade II) was 4 to 19 mitoses per 10 high-power fields (HPF), the presence of brain invasion, or the presence of at least three of these features (‘sheet-like’ growth, hypercellularity, spontaneous necrosis, large and prominent nucleoli, small cells), while criteria for malignant (anaplastic) meningioma (WHO grade III) was frank anaplasia (histology resembling carcinoma, sarcoma, or melanoma) or elevated mitoses with 20 or more mitoses per 10 HPF [27–29]. Additionally, the Ki-67 labelling index was evaluated in all patients. In 42 of 57 patients, mitotic count was evaluated using the mitotic marker phosphohistone-H3.

Statistical Analysis

Based on the results of normality testing by the Kolmogorov–Smirnov test, MTR_{asym} values were compared between enhancing tumours and NAWM by the paired t-test, and $nMTR_{asym}$ values and maximum tumour diameter were compared between patients with benign and atypical meningiomas by Student’s t-test. Correlation between $nMTR_{asym}$ and the Ki-67 labelling index or mitotic count was evaluated by Pearson’s correlation coefficient analysis.

Differences in frequencies of specific imaging features between benign and atypical meningiomas were determined by the chi-square or Fisher’s exact test. Then, $nMTR_{asym}$ and conventional imaging features found to be significant in univariable analysis were further evaluated to compare the diagnostic performance by receiver operating characteristic (ROC) curve. To determine whether inclusion of $nMTR_{asym}$ with conventional MRI features improved the discriminative value of MRI for benign and atypical meningiomas, two different models comprising conventional imaging features which were identified as being significantly associated with atypical meningioma based on univariable analysis with and without $nMTR_{asym}$ (models 1 and 2, respectively) were assessed based on the ROC curve using c-statistics (Harrell’s concordance index) after multivariable logistic regression

analyses. The net reclassification index (NRI) and integrated discrimination improvement (IDI) values of the two models were also calculated to evaluate the increase in discriminative value [30].

Interobserver agreement on $nMTR_{asym}$ in APT images and maximum tumour size in conventional MR images was evaluated by intraclass correlation coefficients (ICC), while that on conventional imaging features was evaluated by Cohen's κ coefficient; ICC and κ values > 0.75 indicated excellent agreement. Statistical analyses were performed using SAS (version 9.2; SAS Institute Ind., Cary, NC, USA), MedCalc (version 9.3.6.0; MedCalc Software, Mariakerke, Belgium), and R (version 3.3.1; R Foundation for Statistical Computing, Vienna, Austria). Statistical significance was set at $P < 0.05$.

Results

Among the 57 included patients, 13 were pathologically diagnosed with atypical meningioma and 44 with benign meningioma (transitional, 18; meningothelial, 15; fibrous, 8; angiomatous, 2; and secretory, 1). None of the patients exhibited malignant meningiomas. While 39 patients exhibited non-skull base tumours (cerebral convexity, 19; parasagittal area, 18; and lateral ventricle, 2), 18 exhibited skull base tumours (posterior fossa, 8; sphenoid ridge, 5; parasellar, 4; and anterior skull base, 1). No patient showed tumour recurrence until February 2017.

There was a significant difference in MTR_{asym} between enhancing tumours (1.84 ± 0.69%) and NAWM (0.10 ± 0.48%; $P < 0.001$). There was also a significant difference in $nMTR_{asym}$ between patients with benign and atypical meningiomas (1.67% vs. 2.46%; $P < 0.001$; Table 1). Figures 2 and 3 present representative cases of benign and atypical meningiomas, respectively. Atypical meningiomas exhibited higher APT-weighted signal intensities than benign meningiomas.

Both Ki-67 labelling index (3.25 ± 2.67) and mitotic count (2.45 ± 2.70) were significantly and positively correlated with $nMTR_{asym}$ (Pearson's correlation coefficients, 0.440 and 0.426, respectively; $P = 0.002$ and 0.017, respectively; Fig 4).

The overall mean maximum tumour diameter was 46.4 ± 17.6 mm, with atypical meningiomas exhibiting significantly greater maximum tumour diameters than benign meningiomas (56.4 ± 23.1 vs. 43.4 ± 14.7 mm; $P = 0.030$). Heterogeneous enhancement and non-skull base location were observed significantly more often in atypical meningiomas than in benign meningiomas. There were no significant differences in the frequencies of other imaging features between the two tumours (Table 1).

ROC curve analysis with $nMTR_{asym}$, heterogeneous enhancement, maximum tumour diameter, and non-skull base location, the $nMTR_{asym}$ showed significantly higher area under the curve (AUC) value than the others. The optimal cutoff value of $nMTR_{asym}$ for predicting atypical meningiomas was >2.19, with sensitivity of 69.2%, and specificity of 84.1%. The values and 95% confidence intervals [CI] of the AUC of the evaluated parameters were as follows: $nMTR_{asym}$, 0.825 (0.701–0.949); heterogeneous enhancement, 0.657 (0.517–

0.798); maximum tumour diameter, 0.671 (0.514–0.828), and non-skull base location, 0.655 (0.517–0.776; Fig 5).

On multivariable logistic regression analysis of the four variables, $nMTR_{asym}$ was an independent imaging biomarker for predicting atypical meningioma (odds ratio, 11.227; P = 0.014; Table 2). On comparison of the predictive power for atypical meningioma of the two multivariable models (model 1 with covariates as maximum tumour diameter, heterogeneous enhancement, and non-skull base location; model 2 with covariates as maximum tumour diameter, heterogeneous enhancement, non-skull base location, and $nMTR_{asym}$) using c-statistics analysis, model 2 exhibited a significantly better diagnostic performance than model 1 (AUC: 0.879 vs. 0.764; P = 0.039). Model 2 also exhibited better performance with NRI of 0.811 (95% CI, 0.272–1.350) and IDI of 0.172 (95% CI, 0.059–0.286) values (Table 2).

Interobserver agreement on $nMTR_{asym}$ and maximum tumour diameter was excellent (ICC values, 0.911 [95% CI, 0.840–0.959] and 0.989 [95% CI, 0.982–0.994], respectively). Interobserver agreement on specific conventional imaging features was also excellent, with κ values of 0.755 to 1.000 for all parameters.

Discussion

Although surgical resection is the main treatment for meningiomas, monitoring or gamma-knife surgery is considered in patients with asymptomatic small meningiomas without pathological diagnosis [31]. Therefore, it is important to identify atypical meningiomas preoperatively. In the present study, we investigated the ability of APT imaging to differentiate between benign and atypical meningiomas. Although preliminary studies have employed APT imaging for evaluation of brain tumours [6, 32], to the best of our knowledge, the present results are the first to describe the feasibility of APT imaging for grading meningiomas. The MTR_{asym} values of both tumours and normal brain tissue are affected by various tissue microenvironment and technical factors. Therefore, we evaluated the diagnostic value of APT imaging based on $nMTR_{asym}$—the difference in MTR_{asym} between tumours and normal brain tissue—because it is minimally affected by non-physiologic factors. Atypical meningiomas exhibited significantly higher $nMTR_{asym}$ than benign meningiomas (2.46% vs. 1.67%), which is in accordance with results of previous studies on APT imaging for grading gliomas that also reported significant increases in signal intensity according to tumour grade [9, 24].

Among the conventional MR features evaluated in the present study, greater maximum tumour diameter, heterogeneous enhancement, and non-skull base location were associated with atypical meningiomas. A recent study also reported the association between tumour volume and histopathological grade of meningioma, which may be attributed to the relatively high proliferative potential of high-grade tumours [18]. Heterogeneous enhancement is associated with heterogeneous distribution of tumour cells, which reflects intratumoural ischemic necrosis, calcification, haemorrhage, and/or cystic changes [18–20]. We also found that non-skull base meningiomas were more likely to be atypical meningiomas, which is in line with previous findings [21–23]. Furthermore, previous studies

have reported the association of anatomical location of meningiomas with not only WHO classification but also higher MIB-1 and Ki-67 labelling indexes [22, 33].

In the present study, however, APT imaging exhibited a better diagnostic performance than conventional MRI in diagnosis of atypical meningiomas. The results of multivariable regression analysis with conventional MRI features and $nMTR_{asym}$ as covariates revealed only high $nMTR_{asym}$ as being a statistically significant predictor of atypical meningiomas. Inclusion of APT imaging parameters with conventional imaging features improved the discriminative value of MRI for benign and atypical meningiomas. Considering that it is relatively difficult to demonstrate a significant difference in AUC analysis of performance models despite an added biomarker being a clinically significant factor, our results indicate the superior discriminative ability of APT imaging for benign and atypical meningiomas. The diagnostic improvement in MRI upon inclusion of APT imaging was also validated by NRI and IDI, which exhibited values greater than zero.

Recent studies on gliomas have demonstrated the positive correlation of APT-weighted signal intensity with Ki-67 labelling and cell proliferation index [9, 10]. In the present study, we also found that APT-weighted signal intensity is positively correlated to Ki-67 labelling index and mitotic count. These results might reflect that high-grade tumours, which exhibit higher proliferative and mitotic activities, have higher densities of cells and, hence, higher concentrations of intracellular proteins and peptides than low-grade tumours.

There are several limitations to the present study. First, there are several previous studies attempting to differentiate typical and atypical/malignant meningiomas by means of diffusion-weighted imaging, which have reported contradictory results [17, 18, 34]. In addition, there are previous studies investigating perfusion MRI in meningioma patients, which reported perfusion MRI findings were correlated with grade of meningioma or Ki-67 labelling index in meningioma [35, 36]. Further studies are required to compare the diagnostic performances of diffusion-weighted imaging, perfusion MRI, and APT imaging in differentiating benign and atypical meningiomas. Second, instead of segmenting entire tumours, ROIs were placed manually in the solid portions of tumours which we thought represented tumour characteristics the most. We chose this method because meningiomas occur near the skull, which is susceptible to field inhomogeneity and consequently may affect APT signals. In addition, the resolution of APT imaging must be improved to achieve adequate coregistration with conventional MRI images and segmentation of the entire tumour. Third, because pathological specimens lose location information during surgical resection, there might have been mismatches between ROIs on images and pathological specimens from resection. Lastly, there were various subtypes of benign meningioma in this study, which might require further investigation to clarify relation between each subgroup and diagnostic performance. On the other hand, there was limited number of atypical meningioma patients and lack of malignant meningioma patient. However, considering the relative rarity of these types of tumours, this result was inevitable.

In summary, atypical meningiomas exhibited significantly higher APT-weighted signal intensities than benign meningiomas. Therefore, APT imaging is a useful imaging biomarker that adds value to conventional MRI for differentiation of atypical and benign meningiomas.

Acknowledgments

The authors thank Ha-Kyu Jeong (Korea Basic Science Institute, Chungcheongbuk-do, Korea) for his valuable suggestions and help with protocol optimization.

Funding:

This study has received funding by the Ministry of Science, ICT & Future Planning (2014R1A1A1002716), and faculty research grants of the Yonsei University College of Medicine (6-2015-0079), and National Institutes of Health (P41 EB015909, R01 CA166171, and R01 EB009731).

Abbreviations and acronyms

MRI	Magnetic resonance imaging
CEST	Chemical exchange saturation transfer
APT	Amide proton transfer
MTR_{asym}	Magnetization transfer ratio asymmetry
$nMTR_{asym}$	Normalized magnetization transfer ratio asymmetry
ROC	Receiver operating characteristic
AUC	Area under the curve
NRI	Net reclassification index
IDI	Integrated discrimination improvement
ICC	Intraclass correlation coefficients

References

1. Ward KM, Aletras AH, Balaban RS. A new class of contrast agents for MRI based on proton chemical exchange dependent saturation transfer (CEST). J Magn Reson. 2000; 143:79–87. [PubMed: 10698648]
2. Wen Z, Hu S, Huang F, Wang X, Guo L, Quan X, Wang S, Zhou J. MR imaging of high-grade brain tumors using endogenous protein and peptide-based contrast. Neuroimage. 2010; 51:616–622. [PubMed: 20188197]
3. Zhou J, Lal B, Wilson DA, Laterra J, van Zijl PC. Amide proton transfer (APT) contrast for imaging of brain tumors. Magn Reson Med. 2003; 50:1120–1126. [PubMed: 14648559]
4. Zhou J, Payen JF, Wilson DA, Traystman RJ, van Zijl PC. Using the amide proton signals of intracellular proteins and peptides to detect pH effects in MRI. Nat Med. 2003; 9:1085–1090. [PubMed: 12872167]
5. Zhou J, Zhu H, Lim M, Blair L, Quinones-Hinojosa A, Messina SA, Eberhart CG, Pomper MG, Laterra J, Barker PB, van Zijl PC, Blakeley JO. Three-dimensional amide proton transfer MR imaging of gliomas: Initial experience and comparison with gadolinium enhancement. J Magn Reson Imaging. 2013; 38:1119–1128. [PubMed: 23440878]
6. Jones CK, Schlosser MJ, van Zijl PC, Pomper MG, Golay X, Zhou J. Amide proton transfer imaging of human brain tumors at 3T. Magn Reson Med. 2006; 56:585–592. [PubMed: 16892186]
7. Tietze A, Blicher J, Mikkelsen IK, Ostergaard L, Strother MK, Smith SA, Donahue MJ. Assessment of ischemic penumbra in patients with hyperacute stroke using amide proton transfer (APT) chemical exchange saturation transfer (CEST) MRI. NMR Biomed. 2013; doi: 10.1002/nbm.3048

8. Wang M, Hong X, Chang CF, Li Q, Ma B, Zhang H, Xiang S, Heo HY, Zhang Y, Lee DH, Jiang S, Leigh R, Koehler RC, van Zijl PC, Wang J, Zhou J. Simultaneous detection and separation of hyperacute intracerebral hemorrhage and cerebral ischemia using amide proton transfer MRI. Magn Reson Med. 2015; doi: 10.1002/mrm.25690
9. Togao O, Yoshiura T, Keupp J, Hiwatashi A, Yamashita K, Kikuchi K, Suzuki Y, Suzuki SO, Iwaki T, Hata N, Mizoguchi M, Yoshimoto K, Sagiyama K, Takahashi M, Honda H. Amide proton transfer imaging of adult diffuse gliomas: correlation with histopathological grades. Neuro Oncol. 2014; 16:441–448. [PubMed: 24305718]
10. Sagiyama K, Mashimo T, Togao O, Vemireddy V, Hatanpaa KJ, Maher EA, Mickey BE, Pan E, Sherry AD, Bachoo RM, Takahashi M. In vivo chemical exchange saturation transfer imaging allows early detection of a therapeutic response in glioblastoma. Proc Natl Acad Sci U S A. 2014; 111:4542–4547. [PubMed: 24616497]
11. Scheidegger R, Wong ET, Alsop DC. Contributors to contrast between glioma and brain tissue in chemical exchange saturation transfer sensitive imaging at 3Tesla. Neuroimage. 2014; 99:256–268. [PubMed: 24857712]
12. Porter KR, McCarthy BJ, Freels S, Kim Y, Davis FG. Prevalence estimates for primary brain tumors in the United States by age, gender, behavior, and histology. Neuro Oncol. 2010; 12:520–527. [PubMed: 20511189]
13. Jung KW, Ha J, Lee SH, Won YJ, Yoo H. An updated nationwide epidemiology of primary brain tumors in republic of Korea. Brain Tumor Res Treat. 2013; 1:16–23. [PubMed: 24904884]
14. Kshettry VR, Ostrom QT, Kruchko C, Al-Mefty O, Barnett GH, Barnholtz-Sloan JS. Descriptive epidemiology of World Health Organization grades II and III intracranial meningiomas in the United States. Neuro Oncol. 2015; 17:1166–1173. [PubMed: 26008603]
15. Pasquier D, Bijmolt S, Veninga T, Rezvoy N, Villa S, Krengli M, Weber DC, Baumert BG, Canyilmaz E, Yalman D, Szutowicz E, Tzuk-Shina T, Mirimanoff RO, Rare Cancer N. Atypical and malignant meningioma: outcome and prognostic factors in 119 irradiated patients. A multicenter, retrospective study of the Rare Cancer Network. Int J Radiat Oncol Biol Phys. 2008; 71:1388–1393. [PubMed: 18294779]
16. Kaur G, Sayegh ET, Larson A, Bloch O, Madden M, Sun MZ, Barani IJ, James CD, Parsa AT. Adjuvant radiotherapy for atypical and malignant meningiomas: a systematic review. Neuro Oncol. 2014; 16:628–636. [PubMed: 24696499]
17. Nagar VA, Ye JR, Ng WH, Chan YH, Hui F, Lee CK, Lim CC. Diffusion-weighted MR imaging: diagnosing atypical or malignant meningiomas and detecting tumor dedifferentiation. AJNR Am J Neuroradiol. 2008; 29:1147–1152. [PubMed: 18356472]
18. Hwang WL, Marciscano AE, Niemierko A, Kim DW, Stemmer-Rachamimov AO, Curry WT, Barker FG 2nd, Martuza RL, Loeffler JS, Oh KS, Shih HA, Larvie M. Imaging and extent of surgical resection predict risk of meningioma recurrence better than WHO histopathological grade. Neuro Oncol. 2016; 18:863–872. [PubMed: 26597949]
19. Kawahara Y, Nakada M, Hayashi Y, Kai Y, Hayashi Y, Uchiyama N, Nakamura H, Kuratsu J, Hamada J. Prediction of high-grade meningioma by preoperative MRI assessment. J Neurooncol. 2012; 108:147–152. [PubMed: 22327898]
20. Lin B-J, Chou K-N, Kao H-W, Lin C, Tsai W-C, Feng S-W, Lee M-S, Hueng D-Y. Correlation between magnetic resonance imaging grading and pathological grading in meningioma: Clinical article. Journal of neurosurgery. 2014; 121:1201–1208. [PubMed: 25148010]
21. Kane AJ, Sughrue ME, Rutkowski MJ, Shangari G, Fang S, McDermott MW, Berger MS, Parsa AT. Anatomic location is a risk factor for atypical and malignant meningiomas. Cancer. 2011; 117:1272–1278. [PubMed: 21381014]
22. Cornelius JF, Slotty PJ, Steiger HJ, Hanggi D, Polivka M, George B. Malignant potential of skull base versus non-skull base meningiomas: clinical series of 1,663 cases. Acta Neurochir (Wien). 2013; 155:407–413. [PubMed: 23318687]
23. Liang RF, Xiu YJ, Wang X, Li M, Yang Y, Mao Q, Liu YH. The potential risk factors for atypical and anaplastic meningiomas: clinical series of 1,239 cases. Int J Clin Exp Med. 2014; 7:5696–5700. [PubMed: 25664093]

24. Zhou J, Blakeley JO, Hua J, Kim M, Laterra J, Pomper MG, van Zijl PC. Practical data acquisition method for human brain tumor amide proton transfer (APT) imaging. Magn Reson Med. 2008; 60:842–849. [PubMed: 18816868]
25. Zhu H, Jones CK, van Zijl PC, Barker PB, Zhou J. Fast 3D chemical exchange saturation transfer (CEST) imaging of the human brain. Magn Reson Med. 2010; 64:638–644. [PubMed: 20632402]
26. Kim M, Gillen J, Landman BA, Zhou J, van Zijl PC. Water saturation shift referencing (WASSR) for chemical exchange saturation transfer (CEST) experiments. Magn Reson Med. 2009; 61:1441–1450. [PubMed: 19358232]
27. Kleihues, P., Cavenee, WK. Pathology and genetics of tumours of the nervous system. IARC Press; Lyon: 2000. International Agency for Research on Cancer.
28. Louis DN, Ohgaki H, Wiestler OD, Cavenee WK, Burger PC, Jouvet A, Scheithauer BW, Kleihues P. The 2007 WHO classification of tumours of the central nervous system. Acta Neuropathol. 2007; 114:97–109. [PubMed: 17618441]
29. Louis DN, Perry A, Reifenberger G, von Deimling A, Figarella-Branger D, Cavenee WK, Ohgaki H, Wiestler OD, Kleihues P, Ellison DW. The 2016 World Health Organization Classification of Tumors of the Central Nervous System: a summary. Acta Neuropathol. 2016; 131:803–820. [PubMed: 27157931]
30. Pencina MJ, D'Agostino RB Sr, D'Agostino RB Jr, Vasan RS. Evaluating the added predictive ability of a new marker: from area under the ROC curve to reclassification and beyond. Stat Med. 2008; 27:157–172. discussion 207–112. [PubMed: 17569110]
31. Kollova A, Liscak R, Novotny J Jr, Vladyka V, Simonova G, Janouskova L. Gamma Knife surgery for benign meningioma. J Neurosurg. 2007; 107:325–336. [PubMed: 17695387]
32. Zhao X, Wen Z, Huang F, Lu S, Wang X, Hu S, Zu D, Zhou J. Saturation power dependence of amide proton transfer image contrasts in human brain tumors and strokes at 3 T. Magn Reson Med. 2011; 66:1033–1041. [PubMed: 21394783]
33. McGovern SL, Aldape KD, Munsell MF, Mahajan A, DeMonte F, Woo SY. A comparison of World Health Organization tumor grades at recurrence in patients with non-skull base and skull base meningiomas: Clinical article. Journal of neurosurgery. 2010; 112:925–933. [PubMed: 19799498]
34. Santelli L, Ramondo G, Della Puppa A, Ermani M, Scienza R, d'Avella D, Manara R. Diffusion-weighted imaging does not predict histological grading in meningiomas. Acta Neurochir (Wien). 2010; 152:1315–1319. discussion 1319. [PubMed: 20428902]
35. Ginat DT, Mangla R, Yeaney G, Wang HZ. Correlation of diffusion and perfusion MRI with Ki-67 in high-grade meningiomas. AJR Am J Roentgenol. 2010; 195:1391–1395. [PubMed: 21098200]
36. Yang S, Law M, Zagzag D, Wu HH, Cha S, Golfinos JG, Knopp EA, Johnson G. Dynamic contrast-enhanced perfusion MR imaging measurements of endothelial permeability: differentiation between atypical and typical meningiomas. AJNR Am J Neuroradiol. 2003; 24:1554–1559. [PubMed: 13679270]

Key points

1. APT imaging is useful for differentiating between atypical and benign meningiomas.
2. Atypical meningiomas exhibited high APT-weighted signal intensity than benign meningiomas.
3. The diagnostic performance of MRI improved with $nMTR_{asym}$ for predicting atypical meningiomas.

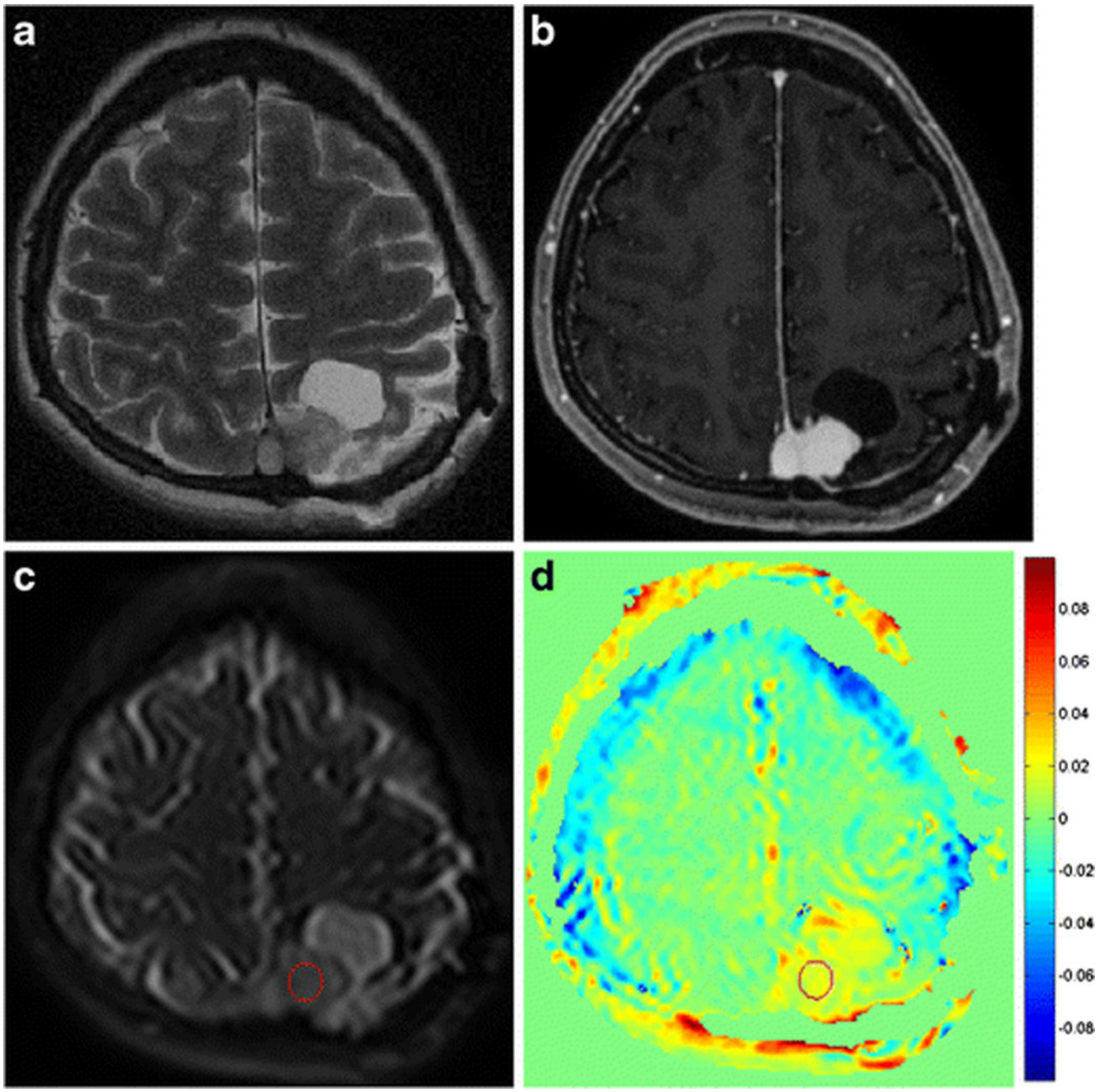

Figure 1.

A region of interest was placed on a raw amide proton transfer (APT) image (c) with equivalent image contrast as a T2-weighted image (a) and a contrast-enhanced T1-weighted image (b). It was then transferred to the processed APT-weighted image (d). By referring to conventional MR images, cystic or necrotic areas could be excluded from ROIs.

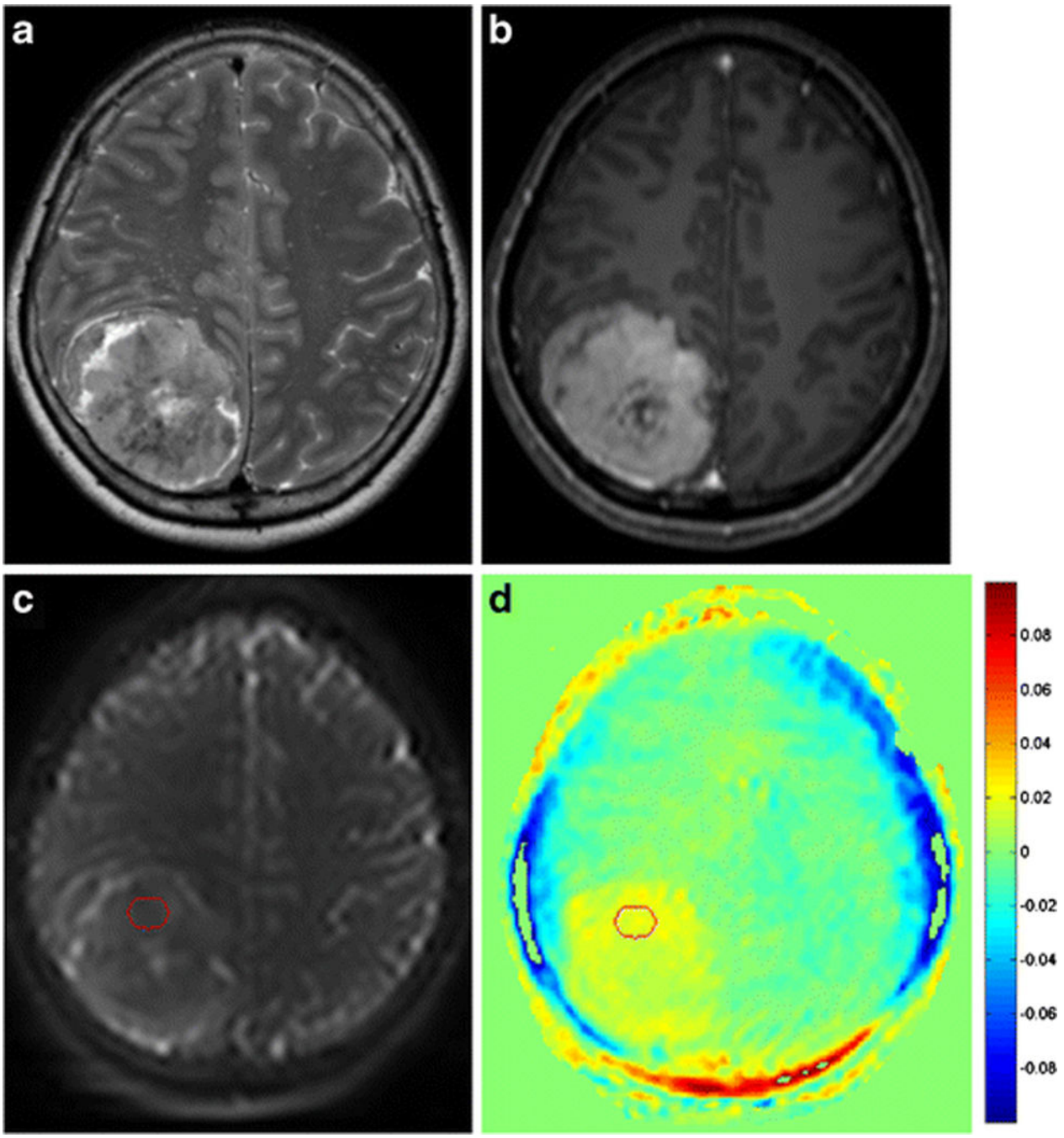

Figure 2.

A 52-year-old female patient with benign meningioma exhibiting low signal intensity on a T2-weighted image (a) and heterogeneous enhancement at the centre on a contrast-enhanced T1-weighted image (b). A ROI was drawn on solid enhancing portion of the tumour on a raw APT image (c) and then transferred to the processed APT-weighted image (d). The normalized magnetization transfer ratio asymmetry value within the enhancing tumour was 1.69 (c).

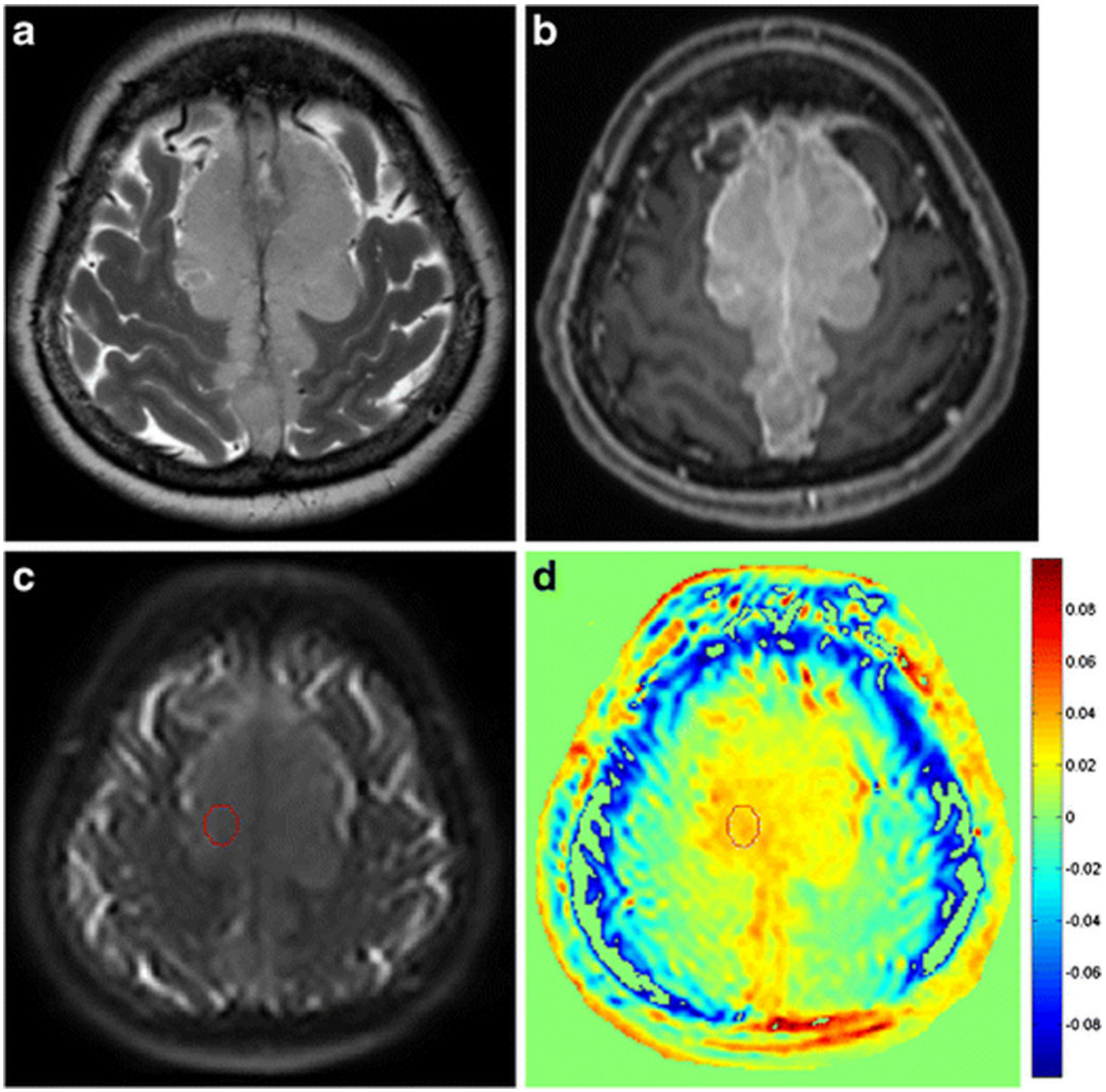

Figure 3.

A 57-year-old female patient with atypical meningioma exhibiting intermediate signal intensity on a T2-weighted image (a) and homogeneous enhancement on a contrast-enhanced T1-weighted image (b). A ROI was drawn on area which showed the highest signal within the tumour on a raw APT image (c) and then transferred to the processed APT-weighted image (d). The normalized magnetization transfer ratio asymmetry value within the enhancing tumour was 3.12 (c).

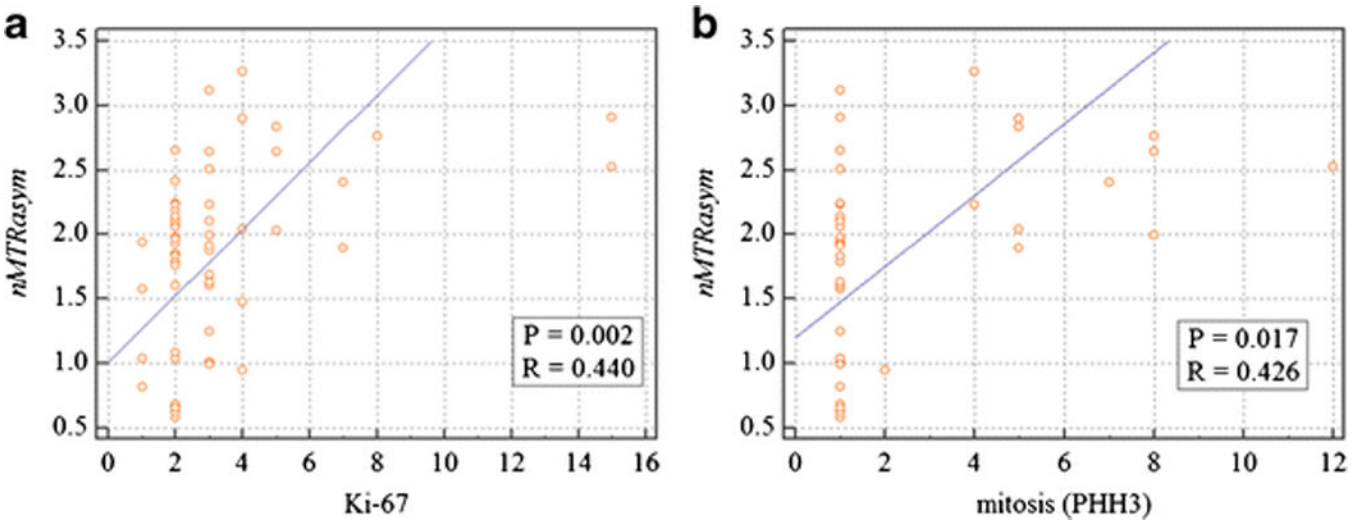

Figure 4.

Correlation of normalized magnetization transfer ratio asymmetry value ($nMTR_{asym}$) with Ki-67 labelling (a) and mitosis (b).

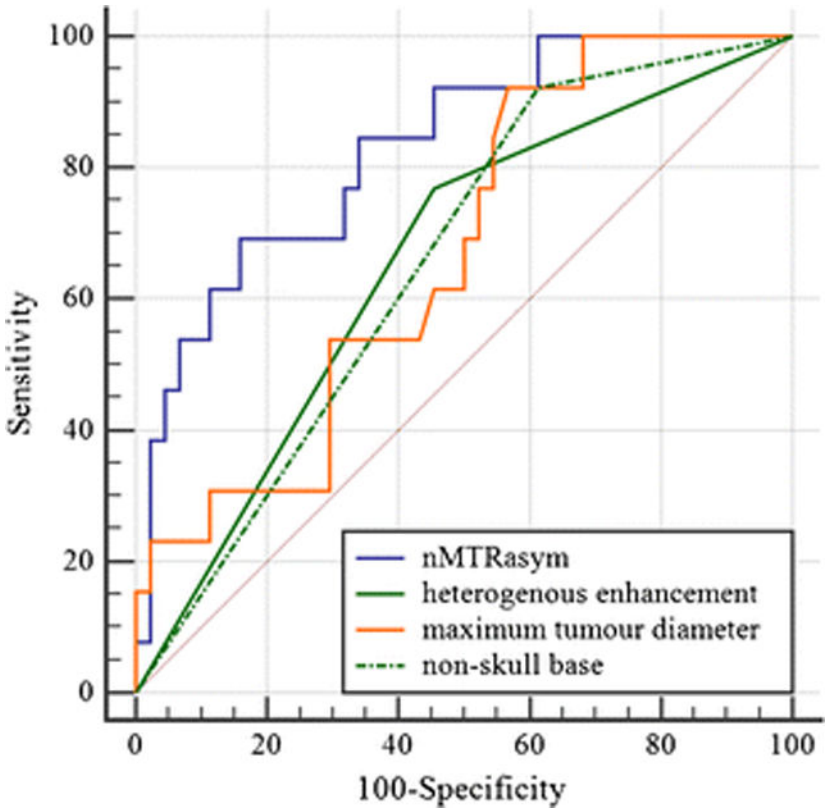

Figure 5.

Receiver operating characteristic curve analysis. Normalized magnetization transfer ratio asymmetry value ($nMTR_{asym}$; area under the curve [AUC], 0.825; 95% confidence interval [CI], 0.701–0.949); heterogeneous enhancement (AUC, 0.657; 95% CI, 0.517–0.798); maximum tumour diameter (AUC, 0.671; 95% CI, 0.514–0.828); non-skull base location (AUC, 0.655; 95% CI, 0.517–0.776).

Table 1

Comparison of Demographic and Clinical Characteristics and Imaging Findings between Patients with Benign and Atypical Meningiomas

	Benign Meningioma (n = 44)	Atypical Meningioma (n = 13)	P value
Age (mean ± SD), years	53.0 ± 11.95	60.0 ± 13.26	0.130
Sex (male)	12 (27.3%)	4 (30.8%)	0.805
$nMTR_{asym}$ (mean ± SD)	1.67 ± 0.64	2.46 ± 0.48	< 0.001
Maximum tumour diameter (mean ± SD), mm	43.4 ± 14.7	56.4 ± 23.1	0.030
Non-skull base location	27 (61.4%)	12 (92.3%)	0.044
T2 hyperintensity	21 (47.7%)	6 (46.2%)	1.000
Peritumoural brain oedema	19 (43.2%)	9 (69.2%)	0.123
Irregular tumour margin	8 (18.2%)	4 (30.8%)	0.440
Heterogeneous enhancement	20 (45.5%)	10 (76.9%)	0.048
Capsular enhancement	8 (18.2%)	1 (7.7%)	0.668
Cystic change	2 (4.5%)	1 (7.7%)	0.547
Reactive hyperostosis	15 (34.1%)	4 (21.1%)	1.000
Skull invasion	10 (22.7%)	3 (23.1%)	1.000
Dural tail sign	29 (65.9%)	6 (46.2%)	0.215

Note—Unless otherwise indicated, data are presented as number of patients (%). P values were calculated using Student's *t*-test for continuous variables and the chi-square or Fisher's exact test for categorical variables. $nMTR_{asym}$ = normalized magnetization transfer ratio asymmetry value.

Table 2

Performance Comparison of Multivariable Logistic Regression Models with and without $nMTR_{asym}$ for Prediction of Atypical Meningioma

	Model 1			Model 2		
Variables	**Adjusted OR**	**95% CI**	**P value**	**Adjusted OR**	**95% CI**	**P value**
Maximum tumour diameter	1.036	0.998–1.084	0.238	1.004	0.958–1.052	0.876
Heterogeneous enhancement	2.581	0.571–14.789	0.571–14.789	1.618	0.282–9.293	0.589
Non-skull base location	5.262	0.577–47.948	0.141	6.953	0.607–1.052	0.119
$nMTR_{asym}$				11.227	1.632–77.241	0.014
AUC*	0.764 (95% CI, 0.633–0.866)			0.879 (95% CI, 0.772–0.954)		
NRI	reference			0.811 (95% CI: 0.272–1.350)		
IDI	reference			0.172 (95% CI: 0.059–0.286)		

Model 1 = maximum tumour diameter + heterogeneous enhancement + non-skull base location

Model 2 = maximum tumour diameter + heterogeneous enhancement + non-skull base location + $nMTR_{asym}$

AUC = area under the receiver operating characteristic curve, CI = confidence interval, IDI = integrated discrimination index, $nMTR_{asym}$ = normalized magnetization transfer ratio asymmetry value, NRI = net reclassification index, OR = odds ratio.

*P = 0.039